Synthesis and Characterization of Colloidal ZnTe/ZnS and ZnTe/ZnSe Quantum Dots

Honors Thesis
Presented to the Department of Physics and Astronomy
University of New Mexico

By:
Gavin Gonzales
May 11, 2019

Supervisor:
Dr. Marek Osiński

Title: Synthesis and Characterization of Colloidal ZnTe/ZnS and ZnTe/ZnSe Quantum Dots

Gavin Gonzales[1,2]
Marek Osiński [1,2]

[1]Department of Physics and Astronomy, University of New Mexico
[2]Center for High Technology Materials, University of New Mexico

Abstract:

Quantum dots (QDs) that emit in the visible spectrum potentially have many biomedical applications, including bioimaging, biosensing, drug targeting, and photodynamic therapy. However, using QDs is significantly limited because they typically contain cadmium, which is cytotoxic and makes FDA approval very unlikely for human treatment. Previous work on biocompatible QDs has focused on indium phosphide and zinc oxide as alternative semiconductor materials. However, these nanoparticles have also been shown to be cytotoxic. High-efficiency luminescent ZnTe core QDs could be a reasonable alternative. Our recent studies of zinc chalcogenide QDs started with synthesis, structural characterization, and investigation of optical properties of ZnTe/ZnSe colloidal QDs that displayed a visible photoluminescence under ultraviolet excitation. The characteristics of ZnTe/ZnS QDs synthesized under different conditions were then compared in order to determine an optimal choice of core/shell thickness for maximum quantum efficiency.

Table of Contents:

Table of Figures:

1. Introduction

1.1. Introduction to quantum dots in biomedical applications.

Quantum dots (QDs) are semiconductor nanocrystals that are 1-100 nm in size and are coated with an organic ligand. "[QDs] exhibit strongly size-dependent optical and electrical properties. The ability to join quantum dots into complex assemblies creates many opportunities for scientific discovery" [Alivisatos 1996]. In a simple scenario, a spherical quantum dot can be thought to be like a simple one-dimensional "particle in a box"; as the size of the sphere decreases in radius, the confined particle has higher separation between its energy states [Guan 2008]. As the size of the particle is reduced, the electronic excitations shift to higher energy [Alivisatos 1996]. This leads to the size of the core nanocrystals having the greatest effect on the wavelength of light that a nanoparticle emits. However, the presence of a shell and the thickness of this shell layer also influence the optical properties of the QDs. The shells coating the core have been found to passivate the surface and increase the quantum efficiency of the particles [Alivisatos 1996], [Guan 2008]. Also, when compared to currently used fluorescent markers in biological imaging such as organic dyes, QDs are more stable against photobleaching [Guan 2008].

QDs emitting in the visible spectrum are of interest for many biomedical applications, including bioimaging, biosensing, drug targeting, and photodynamic therapy [Chatterjee 2008], [Wang 2013]. Luminescent colloidal nanoparticles are promising candidates for visible, color-tunable, biological markers. Because of quantum confinement, the wavelength that certain nanomaterials emit is not completely dependent on their composition or crystallographic structure, but also on the size of the nanoparticles. Most nanoparticles that display these luminescent properties are metal-containing compounds. Among those, cadmium-chalcogenide-core compounds are the most widely used [Tsay 2004], [Law 2009], [Jing 2013], [Zhao 2017]. A large concern with these compounds, however, is their cytotoxicity: unless the cores are tightly coated with a non-toxic (typically containing zinc) shell material, the cadmium chalcogenide cores are dangerous for *in-vivo* biomedical applications because they are toxic to cells [Law 2009], [Wang 2013]. For instance, CdTe/ZnS QDs have been used for imaging of lymph nodes in mice [Zhao 2017].

For *in-vivo* biomedical applications, it is very important to identify compounds with a low cytotoxicity and strong luminescent properties that could replace cadmium-containing cores. Desirable qualities in applications of colloidal nanoparticles are high colloidal stability, small size distribution, high quantum efficiency, and long luminescence lifetime [Wang 2013]. Zinc chalcogenides are a promising core material for biomedical applications because they have similar physical properties to cadmium chalcogenides, but they have been shown to be less cytotoxic. We believe that QDs composed of a zinc chalcogenide core and a zinc chalcogenide shell with a larger bandgap than the core material would have similar properties and be less cytotoxic than the more commonly used alternatives with cadmium-containing cores [Tulsky 2014].

1.2. Introduction to zinc chalcogenide QDs.

Due to its smaller bandgap, zinc telluride (ZnTe) is an attractive material for the QD core. Zinc, in general, is a much less cytotoxic metal than cadmium, and ZnTe has a bandgap that is smaller than other zinc chalcogenides: zinc sulfide (ZnS) and zinc selenide (ZnSe) [Xie 2005], [Guan 2008]. ZnS or ZnSe shells would form type-II heterostructures with the ZnTe cores [Guan 2008], [Sukkabot 2015]. In a type-II QD, both the valence and conduction band in the core are lower (or higher) than in the shell, and this allows type-II QDs to have many novel properties that are fundamentally different from the more commonly researched type-I QDs [Kim 2003], [Xie 2005], [Guan 2008]. ZnTe/ZnSe and ZnTe/ZnS core/shell QDs may produce desirable qualities such as a high quantum yield, narrow size distribution, high colloidal stability and long luminescence lifetime [Wang 2013]. Quicker methods to synthesize ZnTe nanoparticles involve air-sensitive chemicals, and, consequently, require a glove box filled with argon or nitrogen, [Xie 2005], [Guan 2008]. However, a direct aqueous synthesis is also attractive for biomedical applications, although so far it has produced the QDs with smaller quantum yields of 7% [Song 2015]. Other methods using aqueous routes rather than air-sensitive chemicals have different concerns, such as a stronger dependence on pH of the reaction solution, and typically longer synthesis times [Xu 2010], [Patra 2016]. High-efficiency ZnTe core QDs could provide a safer alternative to cadmium chalcogenide core QDs because they have similar physical properties and are less cytotoxic then cadmium chalcogenide cores and can still be coated in zinc chalcogenide shells.

ZnTe/ZnSe and ZnTe/ZnS core/shell QDs form type-II interfaces, with staggered alignment of the conduction and valence band edges. In this type-II alignment, both the valence and conduction band in the core are lower (or higher) than in the shell [Kim 2003],[Xie 2005], [Guan 2008]. The direct bandgap of ZnTe is 2.26 eV, the direct bandgap of ZnSe is 2.7 eV, and the direct bandgap of ZnS is 3.61 eV [Guan 2008], [Lincheneau 2014]. As a result, the effective bandgap in these QDs is smaller than that of either of the constituent core or shell materials. By taking advantage of the type-II band alignment and quantum confinement effects, we could engineer QDs with relatively strong photoluminescence because the wavelength of luminescence may be tuned, and the shell provides an increased quantum efficiency [Alivisatos 1996], [Guan 2008]. For example, 12% quantum efficiency has been reported for ZnTe/ZnSe QDs with the shell thickness of 1.5-3 monolayers [Fairclough 2012], while other authors claimed a typical quantum efficiency of 15% for the ZnTe/ZnSe QDs with the shell thickness of less than 4 monolayers [Guan 2008].

2. Materials and Methods:

2.1. Synthesis methods.

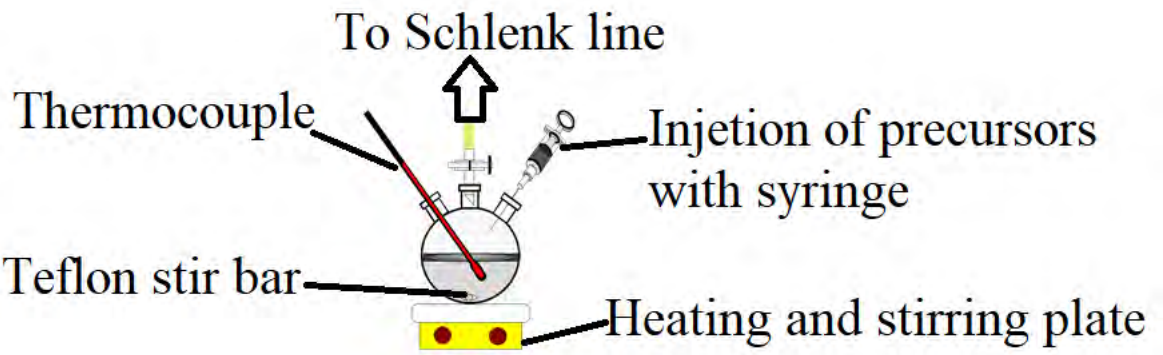

Figure 1: A closed three-neck flask with two septa and a nitrogen adapter. One septum is used to hold the thermocouple, and the other septum is used to inject precursors with a syringe. The three-neck flask sits on the stir plate, has a magnetic stir bar, and is constantly supplied with argon flow from the Schlenk line.

All nanoparticles were synthesized in a three-neck flask attached to a Schlenk line (Figure 1). The Schlenk line allows a controlled supply of argon gas or vacuum to the three-neck flask for the reaction to occur in a controlled and inert environment. The temperature of the reaction was controlled with a temperature controller connected to the flask by a thermocouple, and the heat was suppled through a heating mantle. Furthermore, to mitigate the heat that was lost in the reaction, the three-neck flask and heating mantle were insulated with aluminum foil during the reaction. Every three-neck flask had a Teflon stir bar and was placed on a magnetic stir plate to allow continuous stirring of the reaction.

A glove box with argon gas flow was used in order to handle air-sensitive chemicals. To minimize exposure to air, chemicals were transferred out of the glovebox with a syringe in a plastic bag and injected to the three-neck flask.

2.1.1 SILAR shell calculations.

For the ZnSe shells of the ZnTe/ZnSe QDs, we used a Single Ion Layer Adsorption and Reaction (SILAR) process [Guan 2008]. After the colloidal ZnTe nanoparticles were synthesized, the shells were synthesized by alternating injections of zinc and tellurium precursors at 20 minutes between each injection. The amount of precursor required for each injection was determined by calculating the moles of precursor needed to synthesize a perfect spherical shell of ZnSe over perfectly spherical ZnTe nanoparticles with the same radius [R]. We determined that the number of moles [n] needed to form the i^{th} shell monolayer depended on the densities [ρ], molar masses [μ], and volumes of the materials [V] that make up the core and i^{th} shell monolayers is:

$$n_{shell\_i} = n_{ZnTe} * \frac{\mu_{ZnTe}}{\mu_{ZnSe}} * \frac{\rho_{ZnSe}}{\rho_{ZnTe}} * \frac{V_{shell\_i}}{V_{core}}$$

The thickness [H] of the shells was estimated to be multiples of a unit cell of a zinc blende structure based on the material's lattice parameter [a], and the radius of the shell's monolayer was determined to be the radius of one-unit cell of shell material with a radius calculated from the lattice parameter. These hollow shells were assumed to be perfect spheres [$V = {}^{4}/_{3}\,\pi(R_2^3 - R_1^3)$; $H \equiv R_2 - R_1$] (Figure 2).

Figure 2: An example of the estimation of a ZnTe-nanoparticle core with three ZnSe monolayers with the same thickness.

2.1.2. Instability of ZnTe cores.

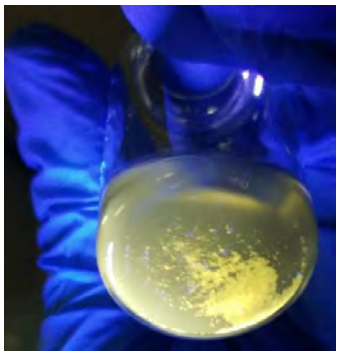

Figure 3: Oxidized ZnTe-nanoparticle cores dispersed in hexanes a week after synthesis under UV Light.

ZnTe-nanoparticle cores are not colloidally stable for extended periods of time alone. This instability manifested itself in the ZnTe-nanoparticle cores quickly oxidizing to zinc oxide and allowing the tellurium powder to precipitate (Figure 3) [Ji 2017]. In order to synthesize a more robust ZnTe core nanoparticle, a shell must be added to improve the colloidal stability as well as for increased control of the photoluminescence.

2.1.3. Experimental workflow.

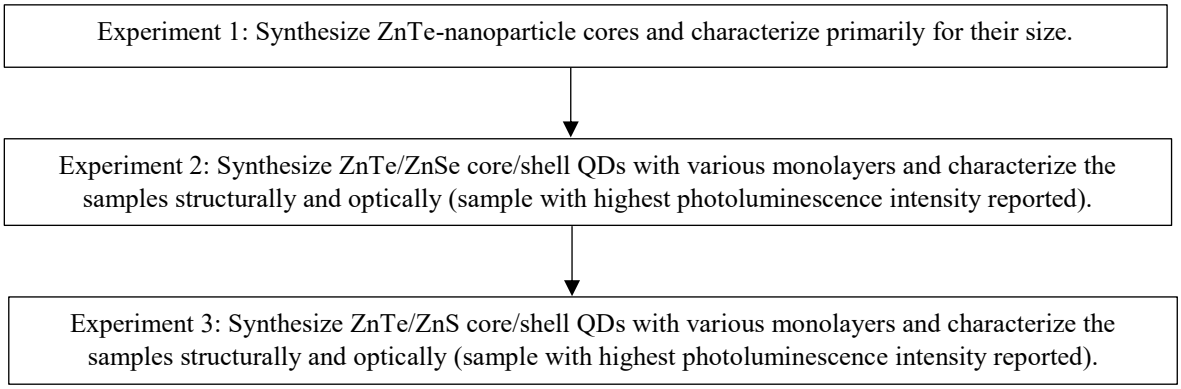

Figure 4: Experimental workflow for the development of the reported synthesis procedures.

For the experiment, a synthesis of the ZnTe cores was first created. The cores were tested with transmission electron microscopy to determine their radius to be 1.85 nm to 2.5 nm. After, the ZnTe/ZnSe core/shell QDs were synthesized and tested with various monolayers, and ZnTe/ZnSe QDs with one, two and three shell monolayers were determined to be the best product. Next, ZnTe/ZnS QDs were synthesized with one, two and three shell monolayers, and the ZnTe/ZnS QDs with three shell monolayers were determined to be the best product.

2.2.1. Materials (ZnTe/ZnSe QDs).

Tellurium powder (Te, 99.8%), selenium powder (Se, 99.8%), oleic acid (95%), trioctylphosphine (TOP, 90%), oleylamine (OA, 98%), 1-octadecene (ODE, 90%), butanol, methanol, and hexanes were purchased from Sigma-Aldrich, USA, and zinc acetate was purchased from Mallinckrodt. All chemicals were used as received without purification.

2.2.2. Synthesis of ZnTe nanoparticles and ZnTe/ZnSe core/shell QDs.

Our synthesis method for the ZnTe-nanoparticle cores required a 0.1 M trioctylphosphine tellurium solution (TOPTe) as a tellurium precursor, diethylzinc ($ZnEt_2$) as a zinc precursor, 1-octadecene (ODE) as a reaction solvent with a high boiling point, and oleylamine (OA) for an organic ligand coating that also functioned as a stabilizing surfactant [Matteucci 2006]. The ZnSe shell required a 0.1 M zinc acetate solution prepared from zinc acetate and oleic acid in ODE, and a 0.1M solution of selenium in TOP.

In our synthesis, OA and ODE were heated to 110 °C for one hour in a three-neck flask connected to a Schlenk line under continuous argon flow. Then, the reaction was heated to 285 °C, and a $ZnEt_2$/TOPTe solution was injected at slightly above the boiling point of the TOP. The temperature immediately dropped to 270 °C. After a two-minute reaction, ZnTe nanoparticles were produced that luminesced bright yellow under a 365 nm ultraviolet light while the ZnTe nanoparticles were still under argon in the three-neck flask. Then, the temperature was reduced to 240 °C. First, the zinc shell precursor was injected. After letting the reaction occur for 20 minutes, the selenium precursor was injected, and this reaction progressed for another 20 minutes. Then, the nanoparticles were cooled and washed in a mixture of

methanol and butanol. Finally, the nanoparticles were stored in hexanes, and appeared to luminesce a duller yellow under the ultraviolet lamp (365 nm). The synthesis, washing, and storage procedures were developed from the procedures of [Xie 2005], [Zhang 2006], [Guan 2008], [Tulsky 2014]. The methods were first reported in [Gonzales 2018].

2.2.3. Synthesis of colloidal ZnTe nanoparticle cores.

Figure 5: Three-neck flask with ZnTe-nanoparticle cores under UV light shortly after reaction.

In a typical synthesis, OA and ODE were heated to 110 °C under continuous and moderate stirring. The solvents were left to degas for an hour in a 50-mL three-neck flask connected to a Schlenk line placed under argon flow. Then the three-neck flask was heated to 285 °C (slightly above the boiling point of TOP). While the flask was being heated, a solution on TOPTe/$ZnEt_2$ was prepared in the argon-filled glovebox, with $ZnEt_2$ and a 0.1 M TOPTe solution. The TOPTe/$ZnEt_2$ solution was injected into the three-neck flask, and the temperature was maintained at 270 °C for two minutes to permit ZnTe nanoparticles to form. This reaction was calculated to produce ZnTe cores with a 4 nm diameter. After the reaction, the nanoparticles in the three-neck flask emitted visible light when excited by a 365 nm ultraviolet light source (Figure 5).

2.2.4. Synthesis of ZnSe shells.

Figure 6: Three-neck flask with ZnTe/ZnSe QDs with two shell monolayers shortly after the reaction under UV light.

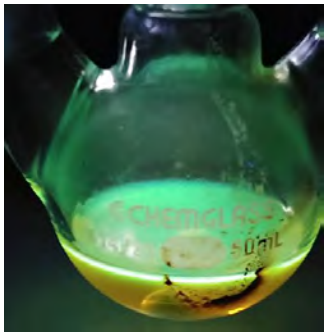

Figure 7: Three-neck flask with ZnTe/ZnS with three shell monolayers shortly after the reaction under UV light.

After the three-minute reaction for the cores, the temperature in the three-neck flask was lowered to 240 °C. Once the flask was at 240 °C, the 0.1M zinc oleate shell precursor was injected, and the reaction proceeded for 20 minutes. Then, the 0.1M TOPSe shell precursor was injected, and the reaction continued for another 20 minutes. Subsequently, the flask was cooled to room temperature, and the nanoparticles were washed. The ZnTe/ZnSe QDs in the three-neck flask emitted visible blue-green when excited with a 365 nm ultraviolet light source (Figure 6 and Figure 7).

2.2.5. Washing of ZnTe/ZnSe core/shell QDs.

Figure 8: Washed ZnTe/ZnSe QDs in centrifuge tube after washing before being dispersed in hexanes.

Figure 9: ZnTe/ZnSe QDs in a scintillation vial with three shell monolayers dispersed in hexanes under UV light.

The excess OA and ODE were removed through three stages of washing in a two-parts methanol and one-part butanol. The contents of the three-neck flask were added to six 10-mL centrifuge tubes with the mixture of methanol and butanol, and the nanoparticles were centrifuged at 4000 rpm for five minutes. The nanoparticles were washed three times (Figure 8). Finally, the ZnTe/ZnSe QDs were stored in hexanes in a 20-mL scintillation vial. In the scintillation vial, the QDs luminesced a visible blue-green when excited with a 365 nm ultraviolet light source (Figure 9).

2.3.1. Materials (ZnTe/ZnS QDs).

Tellurium powder (Te, 99.8%), sulfur powder (S, 99.8%), oleic acid (OlA, 95%), trioctylphosphine (TOP, 90%), oleylamine (OA, 98%), 1-octadecene (ODE, 90%), acetone, methanol, and hexanes were purchased from Sigma-Aldrich, USA, and zinc acetate was purchased from Mallinckrodt. All chemicals were used as received without purification.

2.3.2. Synthesis of ZnTe/ZnS core/shell QDs.

ZnTe nanoparticles were synthesized by a hot injection method into a solution of an organic ligand that functioned as a coordinating solvent oleylamine (OA) and a high boiling point reaction solvent 1-octadecene (ODE) under an inert argon environment. For our ZnTe core precursors, we used a 0.1 M solution of tellurium powder dissolved in trioctylphosphine (TOPTe) for the tellurium precursor and diethylzinc ($ZnEt_2$) for the zinc precursor. Then, for the ZnS shell we created a zinc oleate precursor of 0.17 M zinc acetate dissolved in (OlA), OA and ODE, and a sulfur precursor of 0.22M sulfur powder dissolved in ODE.

In preparation for the synthesis, a three-neck flask was connected to the Schlenk line under argon flow. In this flask, zinc acetate was heated with OlA, OA and ODE to form the zinc shell precursor. After we added these precursors, we heated the flask to 250˚C with medium stirring. After this precursor was heated to 250˚C, it was cooled to 60˚C until it was ready for injection. Also, at this time, another three-neck flask was connected to the Schlenk line under argon flow. In this flask, we prepared the sulfur shell precursor, sulfur powder, in ODE by heating the solution to 200˚C and then cooling it to room temperature until it was needed for injection.

In our synthesis, OA and ODE were mixed in a three-neck flask at medium stirring for one hour at 110˚C with a continuous argon flow to allow the flask to degas. After this hour, we further degassed the flask by switching the argon flow to vacuum for five minutes. After this time, the vacuum flow was switched to argon, and the flask was heated to 285˚C. While the flask was heating, in the glovebox, a solution of $ZnEt_2$/TOPTe was prepared in a syringe. Once the flask was at 285˚C, the syringe was transferred out of the glovebox to the Schlenk line hood, and the solution was injected into the three-neck flask. The temperature of the flask immediately dropped to 270˚C. After a two-minute reaction at this temperature, ZnTe cores were produced, and the flask was cooled to 240˚C.

Before the ZnS shell synthesis, another three-neck flask was connected to the Schlenk line under argon flow. Zinc acetate was added to the flask and mixed with OlA, OA and ODE. The flask was heated to 250 ºC with stirring to form zinc oleate. The flask was then cooled to 60 ºC until it was ready for injection. At the same time, a third three-neck flask was connected to the Schlenk line under argon flow. In this flask, to prepare the sulfur shell precursor, sulfur powder in ODE was heated to 200 ºC and then cooled to room temperature until it was ready for injection.

At this point in time, for every desired monolayer, zinc shell precursor was injected to the flask followed by sulfur shell precursor, in a 1:2 stoichiometric ratio to synthesize one

monolayer, and the reaction proceeded for 15 minutes. After each 15-minute reaction, this process could be repeated to add another monolayer, or the flask was cooled to room temperature to wash the core/shell QDs. The synthesis, washing, and storage procedures were developed from the procedures of [Guan 2008], [Qian 2009], [Akins 2010], [Lincheneau 2014], [Plumley 2014], [Tulsky 2014], [Sukkabot 2015]. The methods were first reported in [Gonzales 2019].

2.3.3. Synthesis of colloidal ZnTe nanoparticle cores with ZnS shells.

Figure 10: Three-neck flask with ZnTe/ZnS QDs with two shell monolayers under UV light shortly after the reaction.

Figure 11: Three-neck flask with ZnTe/ZnS QDs with three shell monolayers under UV light shortly after the reaction.

The colloidal ZnTe nanoparticle cores of 5 nm were synthesized in the same way as described in Section 2.2.3. After the two-minute reaction for the cores, the temperature in the three-neck flask was dropped to 240 °C. Once the flask was at 240 °C, a 0.17M zinc oleate shell precursor was injected followed by a 0.22 M sulfur shell precursor, and the reaction proceeded for 15 minutes. This series of injections of precursors was repeated at increasing volumes, based on the currently estimated radius of the particle, to synthesize each subsequent shell monolayer. Finally, the flask was cooled to room temperature, and the QDs were washed. In the three-neck flask before washing, the QDs luminesced a visible yellow-orange when excited with a 365 nm ultraviolet light source (Figure 10 and Figure 11).

2.3.4 Washing of ZnTe/ZnS core/shell QDs.

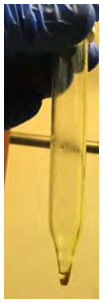

Figure 12: Washed ZnTe/ZnS QDs in centrifuge tube after washing before being dispersed in hexanes.

Figure 13: ZnTe/ZnS QDs in a scintillation vial with three shell monolayers dispersed in hexanes under UV light.

The excess OA, OlA and ODE were removed through several stages of washing in five-parts acetone and one-part methanol. The contents of the three-neck flask were added to six 10-mL centrifuge tubes with the mixture of acetone and methanol, and the QDs were centrifuged at

4000 rpm for five minutes. The nanoparticles were washed three times (Figure 12). Finally, the ZnTe/ZnS QDs were stored in hexanes in a 20-mL scintillation vial. In the scintillation vial, the QDs luminesced a visible and opaque yellow-orange color when excited with a 365 nm ultraviolet light source (Figure 13).

3. Results

3.1 Structural characterization.

To understand the properties of the synthesized QDs, we characterized their structural and optical properties and distinguished the products of the synthesis past their material composition. For our structural characterization, we used Dynamic Light Scattering (DLS) and Transmission Electron Microscopy (TEM) to understand the size and size distribution of the QDs. Also, X-Ray Diffraction (XRD) characterized the size of the particles and the molecular structure of the QDs' crystal lattice. Thermogravimetric Analysis (TGA) was used to determine the total percentage mass of the washed product, and Differential Scanning Calorimetry (DSC) was used to measure the heat required to increase the temperature of the QDs, during the TGA process. After the structural characterization, the QD synthesis and the quality of the washed QDs' could be determined.

3.1.1. Dynamic Light Scattering.

Dynamic light scattering (DLS) was measured using the Wyatt Technology DynaPro Titan instrument. For DLS, the hydrodynamic radius is a spherical equivalent radius of a hard sphere diffusing at the same rate as the particle of interest. In our case, the measured hydrodynamic radius includes the oleylamine coating of the QDs, so the radii obtained by DLS should be larger than the values observed using TEM [Wyatt Technology Corporation 2010] The hydrodynamic size of the ZnTe/ZnSe and ZnTe/ZnS QDs coated in oleylamine determined by DLS was compared to the size of the nanoparticles measured through TEM.

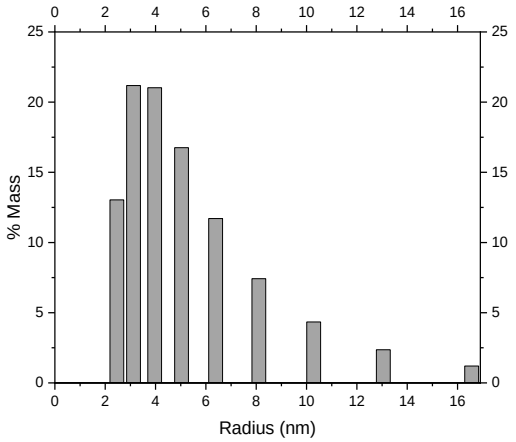

Figure 14: DLS results show the hydrodynamic size distribution of ZnTe/ZnS QDs.

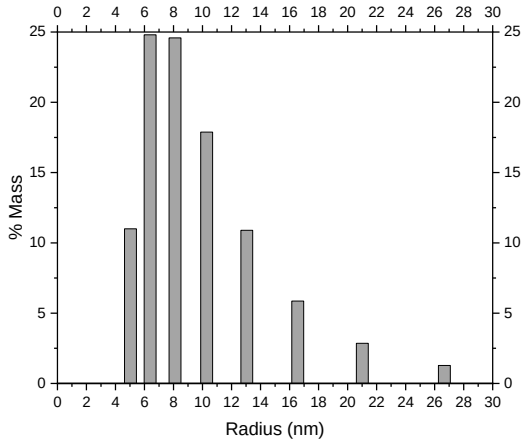

Figure 15: DLS results show the hydrodynamic size distribution of ZnTe/ZnSe QDs.

DLS showed that the distribution of the QDs is monomodal and polydisperse because only one peak is resolved, with most of the values within 5 times the size of the smallest particle [Wyatt Technology Corporation 2010], [Hackley 2015]. Both samples had a hydrodynamic diameter between 6-18 nm (Figures 14 and 15). The hydrodynamic diameter would be the spherical equivalent diameter of a hard sphere diffusing at the same rate as the particle of interest, and this calculation included the hydration or solvent layer that surrounded the particles. In order to make the QDs from the synthesis more monodisperse, the synthesis and washing procedures may be changed to increase the homogeneity of the QDs and remove most of the organic coating and improve the subsequent characterization.

3.1.2. Transmission Electron Microscopy.

TEM measurements of the QDs stored in hexanes were taken with the JEM 2010F electron microscope. The ZnTe/ZnSe QDs were prepared on a copper TEM grid by placing two drops of water on the grid, and then two drops of the ZnTe/ZnSe QDs in hexanes. The ZnTe/ZnS QDs were prepared on a copper TEM grid by placing two drops of ethanol on the grid, and then two drops of the ZnTe/ZnS QDs in hexanes.

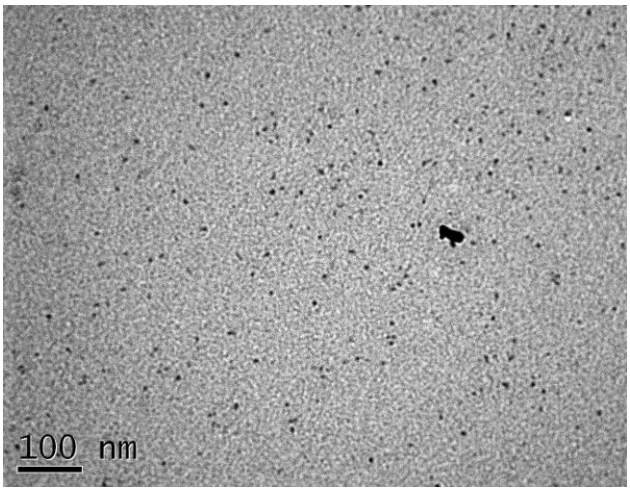

Figure 16: TEM image at low magnification of ZnTe/ZnS QDs. Scale of 100 nm.

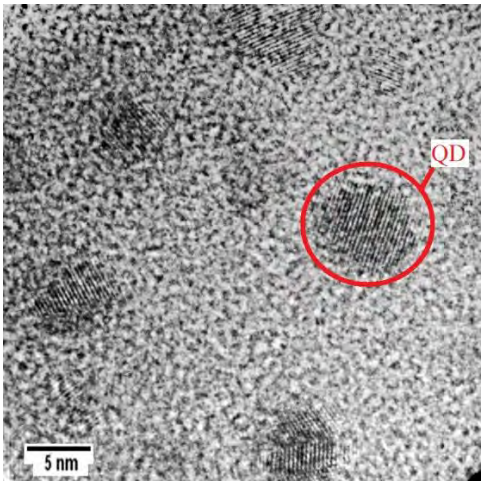

Figure 18: TEM image at high magnification of ZnTe/ZnSe QDs. Scale of 5 nm.

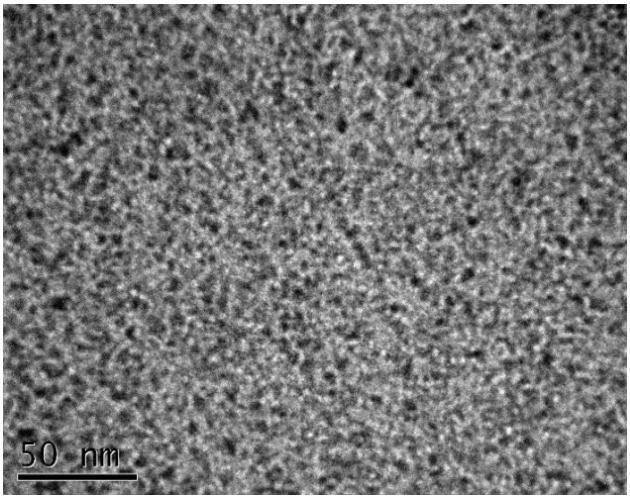

Figure 17: TEM image at low magnification of ZnTe/ZnS QDs. Scale of 50 nm.

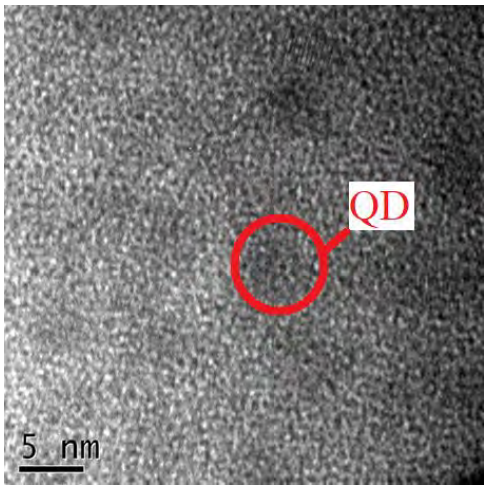

Figure 19: TEM image at high magnification of ZnTe/ZnS QDs. Scale of 5 nm.

The ZnTe/ZnS QDs and ZnTe/ZnS QDs had a diameter of 6-8 nm (Figures 16, 17, 18, and 19). The resolution of the images can be improved by changing the synthesis and washing procedure of the QDs to further remove excess organic coating. The highest resolution image shows lattice fringing in the QDs and diffraction caused by the presence of a crystal lattice in the QDs from each synthesis (Figures 18 and 19).

3.1.3. Energy Dispersive X-ray Spectroscopy.

Energy Dispersive X-ray Spectroscopy (EDS) measurements of the QDs stored in hexanes were taken with the JEM 2010F electron microscope. In EDS measurements, the x-rays are emitted when the sample is bombarded by an electron beam. The relative intensity and energy of the lines in EDS spectrum are used to determine the elemental composition of the sample. The ZnTe/ZnSe QDs were prepared on a copper TEM grid by placing two drops of water on the grid, and then two drops of the ZnTe/ZnSe QDs in hexanes. The ZnTe/ZnS QDs were prepared on a copper TEM grid by placing two drops of ethanol on the grid, and then two drops of the ZnTe/ZnS QDs in hexanes.

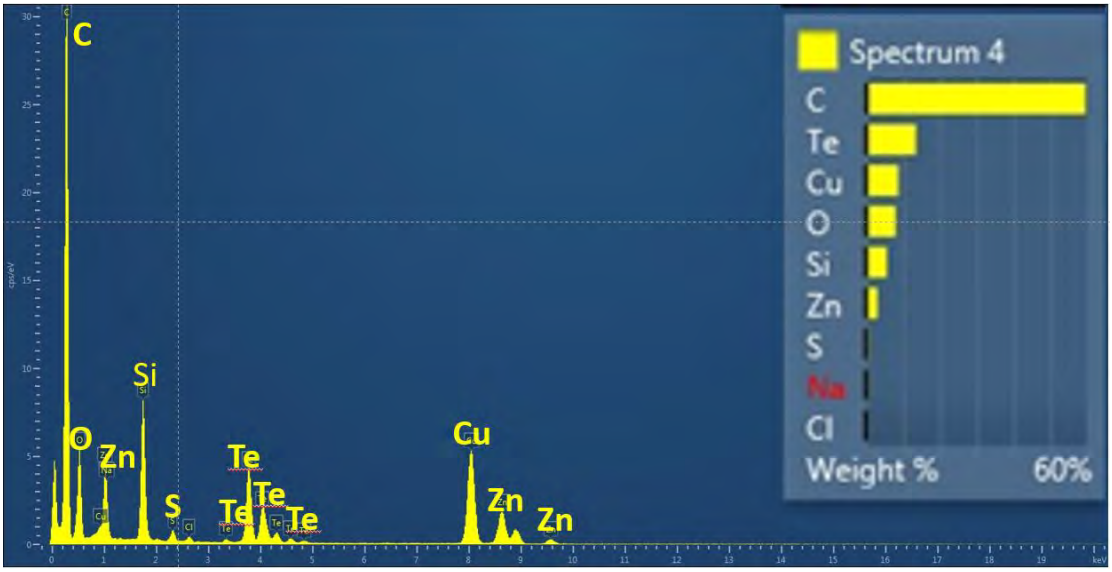

Figure 20: Elemental analysis of ZnTe/ZnS QDs.

The material with the dominant peak is carbon. The high amounts of carbon come from the copper grid used for the characterization which was coated in carbon, and the excess organics on the surface of the quantum dots. Zinc, tellurium and sulfur are peaks that appear from the sample (Figure 20).

3.1.4. X-ray Diffraction.

Crystallographic structure of the ZnTe/ZnSe and ZnTe/ZnS QDs in hexanes was measured using Rigaku X-ray diffraction system. Colloidal QDs dispersed in hexane were tested. After the tests, the Scherrer equation was used to estimate the size of the quantum dots.

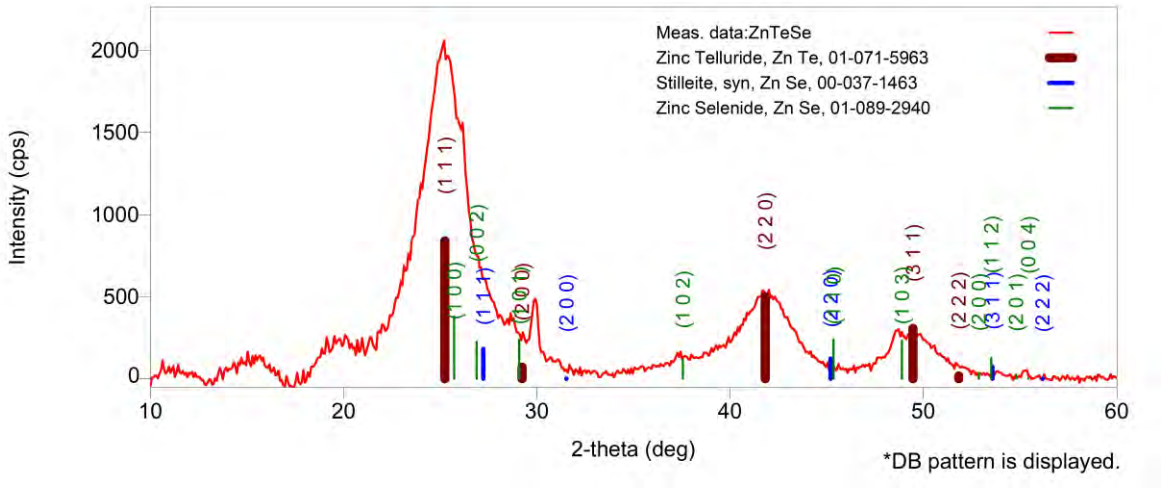

Figure 21: Intensity of X-ray diffraction from ZnTe/ ZnSe QDs.

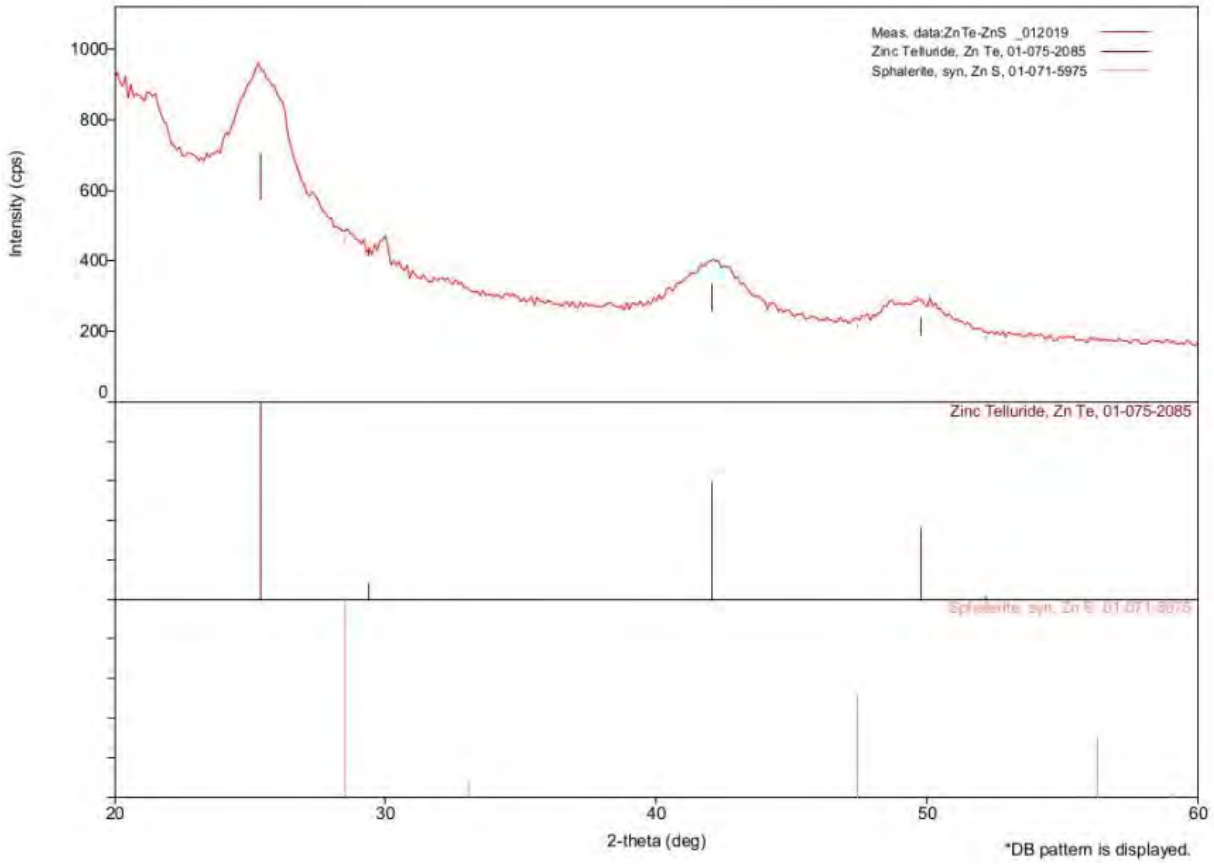

Figure 22: Intensity of X-ray diffraction from ZnTe/ZnS QDs.

These XRD results are indicative of ZnTe/ZnSe and ZnTe/ZnS QDs. The main peak at approximately 27 degrees corresponds to cubic ZnTe. The leftmost peak of the graph that slopes

downward to the first ZnTe peak corresponds to the presence of organic ligands in the solution (Figure 21 and 22). The main peak at approximately 25 degrees corresponds to ZnTe. The ZnTe/ZnSe QDs had cubic ZnSe peaks located at 29 degrees, 37 degrees and 58 degrees (Figure 21). The ZnTe/ZnS QDs had wurtzite ZnS peaks located at 29 degrees and 47 degrees. Finally, in the stretch from 40-50 degrees, a broad peak corresponds to ZnTe at the two edges of the peak with a ZnS peak in the middle (Figure 22).

The broadening of the XRD lines is consistent with the nanocrystal size ranging from 3 nm to 6 nm, and there is still a large organic layer as seen in the other results. These results indicate that the approximate size of the particles is 6 nm and that there is 93% ZnTe and 7% ZnS. But these amounts are only approximate because the material was not sufficiently washed and because too many excess organics were present. In order to better model the diffraction profile, we will need to improve our washing procedure to remove contamination from organic ligands.

3.1.5. Thermogravimetric Analysis and Differential Scanning Calorimetry.

We determined the total percentage of ZnTe/ZnS QDs in our washed product with thermogravimetric analysis (TGA) and differential scanning calorimetry (DSC). This technique allowed us to see the materials response to temperature changes such as mass change or thermal change. TGA/DSC was done with a Netzsch STA 449 F1 Jupiter apparatus. TGA measures the change in mass of the sample as the temperature increases, and it is assumed the mass loss is due to the evaporation of the organics bound to the surface of the QDs. DSC measures the amount of energy required to change the temperature as the temperature increases, and this can also be used to verify that the mass loss is associated with the evaporation of organics. The QDs were dried before the measurement to remove the hexanes and the solid QDs coated with oleylamine were tested.

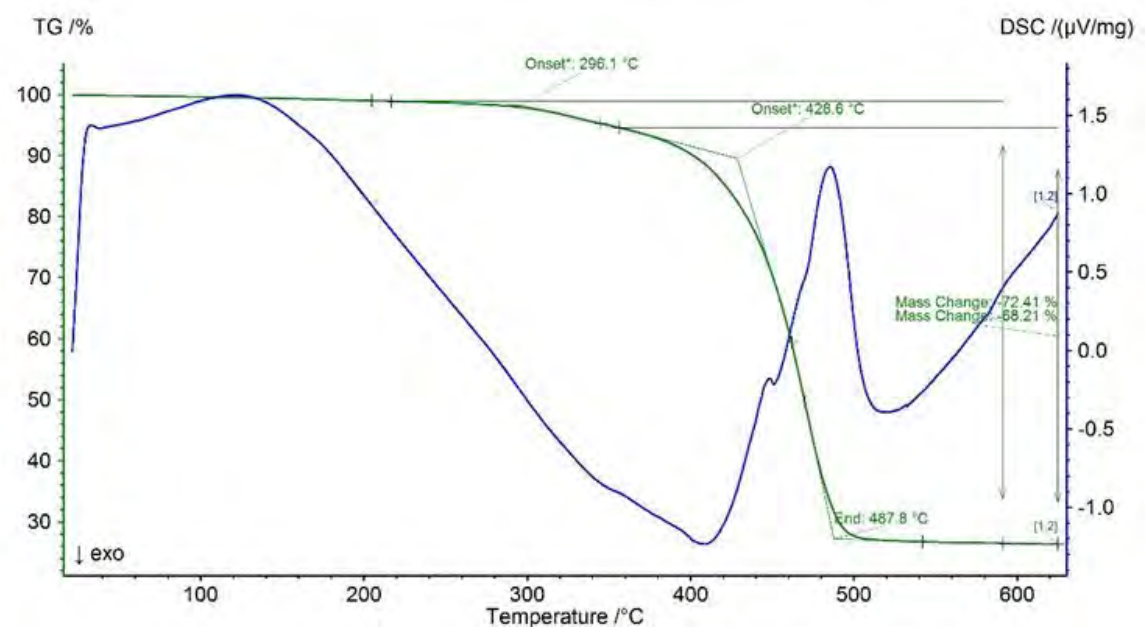

Figure 23: Change in mass as a function of temperature (green line – TG%) and energy required to change temperature as a function of temperature (blue line – DSC).

Most of the product are not ZnTe/ZnS QDs from the synthesis but the organic matrix of bound and non-bound ligands plus possible solvent (Figure 23). However, the mass loss temperature is high compared to what would be expected of oleylamine and can be attributed to the loss of the ligand/organic matrix as judged by the strong endothermic peak from DSC. The higher than expected temperature of the main mass loss stage is possible due to the presence of bound oleate ligand used during deposition of ZnS shell.

3.2 Optical characterization.

Characterizing the optical properties of the QDs was important to understand how the QDs will respond to optical excitation. First, the absorption of the QDs was measured in order to predict what wavelength of light they will respond to and determine a standardized concentration. Next, the QDs were characterized for their photoluminescence (PL), scanning a range of emission wavelengths scanning from 350-750 nm at a fixed excitation wavelength, and photoluminescence-excitation (PL-E), scanning a range of excitation wavelengths at a fixed emission wavelength. We preformed this analysis, in order to determine the intensity of the light emitted from the QDs through a range of wavelengths. Furthermore, PL and PL-E ultimately determine the wavelength of light that emitted the peak intensity of light from the QDs. Finally, the wavelength that produced the highest intensity peak of the PL characterization was tested in a quantum yield (QY) measurement in order to determine the PL quantum efficiency of all QDs; we completed this characterization by using the ratio between the numbers of photons emitted to the number of photons absorbed. The optical characterization is valuable in order to determine the quality of the QDs from each synthesis.

3.2.1. Spectrophotometry.

A Cary 5000 UV/Vis/NIR spectrophotometer was used for absorption measurements. UV absorption peaks were observed for ZnTe nanoparticles, ZnTe/ZnSe and ZnTe/ZnS QDs dispersed in hexanes. The cuvette used had an internal width of 1 cm. These measurements relate the ratio of incident to emitted intensity to the concentration of a colloidal sample via Beer-Lamberts law [$log\frac{I_0}{I} = \varepsilon LC$]. Because the different QDs had different amounts of organics in the washed product, the absolute concentration of the QDs was not determined. However, the absorption measurements were valuable to optimize the photoluminescence measurements, because they provided an indication of relative concentration of QDs between different characterization techniques. Furthermore, this indicated the wavelengths of light that the particles would interact with and helped determine the excitation wavelengths that should be used for photoluminescence measurements.

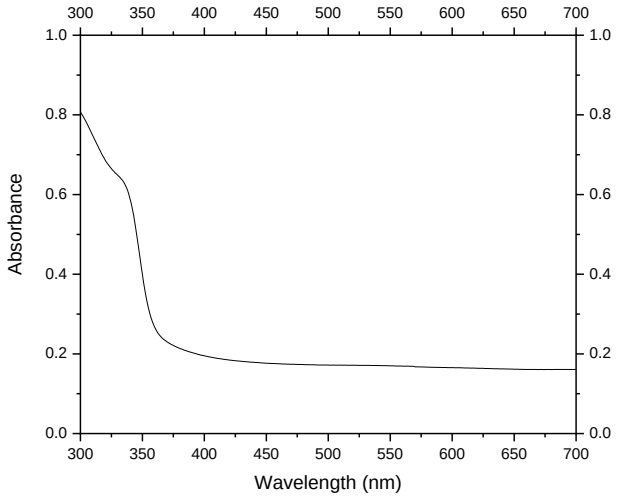

Figure 24: Absorption spectrum of ZnTe nanoparticle cores from 300-700 nm.

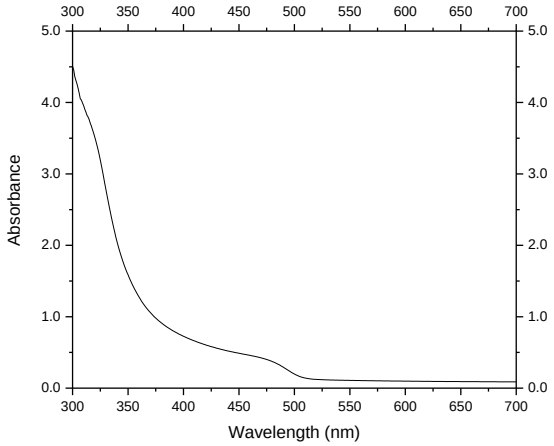

Figure 25: Absorption spectrum of ZnTe/ZnSe QDs from 300-700 nm.

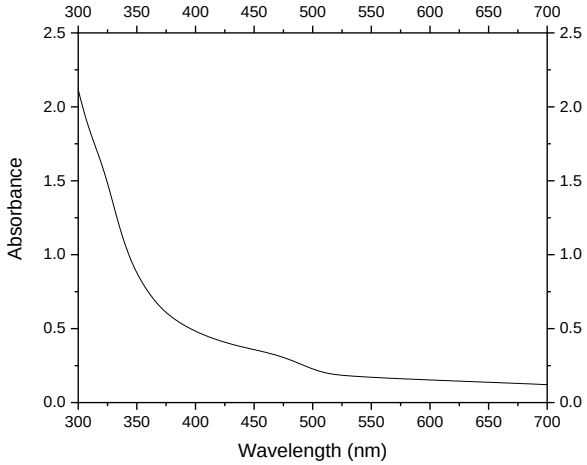

Figure 26: Absorption Spectrum of ZnTe/ZnS QDs from 300-700 nm.

After the synthesis, a series of serial dilutions was conducted to determine the optimal dilution of the particles for the photoluminescence measurements. The ZnTe nanoparticles showed absorption peaks at 332 nm with 0.6 absorbance, and this sample did not absorb much light longer than ultraviolet wavelengths based on the absorbance plateau of 0.2 (Figure 24). The ZnTe/ZnSe QDs showed absorption peaks at 320 nm and 475 nm with 0.6 absorbance (Figure 25). The ZnTe/ZnS QDs had a peak absorbance of 0.6. The two main shoulders of the ZnTe/ZnS QDs appear at 400 nm and 475 nm (Figure 26). These results indicated that the nanoparticles were absorbing ultraviolet light. These wavelengths were the first wavelengths tested for photoluminescence measurements, but ultimately the desired excitation wavelength for photoluminescence measurements was determined from a photoluminescence-excitation scan.

3.2.2. Spectrofluorometry.

A Fluorolog-3 spectrofluorometer from Horiba Jobin Yvon was used for photoluminescence excitation (PL-E) spectroscopy, photoluminescence (PL) spectroscopy, and quantum yield (QY) measurement. The measurements were done with excitation and emission slit width of 2 nm; however, in the image of ZnTe nanoparticles, a 4 nm emission slit width was used. The cuvette used was 1 cm in internal width. The ZnTe nanoparticles, ZnTe/ZnSe and ZnTe/ZnS QDs were tested as they were stored in hexanes. For these measurements, different sample holders were used on the Fluorolog-3. Photoluminescence and photoluminescence-excitation measurements at room temperature were done with a single sample holder; photoluminescence measurements at different temperatures were done with a Horiba Scientific Peltier Sample Cooler attachment, and the quantum efficiency measurements were done with an integrating sphere attachment. PL-E measurements scanned the emission intensity at a range of excitation wavelengths with the emission parked at a single wavelength. PL measurements scanned the emission intensity of the sample at a range of emission wavelengths with a fixed excitation wavelength. Quantum yield measurements were done with a Microsoft Excel script

that measured the intensity of emission at a range of emission wavelengths with a fixed excitation wavelength.

From these measurements, the type of emission spectrum may then be determined in order to understand emission process observed in the sample. In the photoluminescence measurements, we would expect to see Stokes photoluminescence when a photon is absorbed, exciting an electron-hole pair, which then relaxes to a lower energy state before the radiative recombination process results in emission of a Stokes-shifted photon. Alternatively, there can be Raman scattering where "a laser photon bounces off a molecule and loses a certain amount of energy that allows the molecule to vibrate (Stokes process). The scattered photon is therefore less energetic, and the associated light exhibits a frequency shift. The various frequency shifts associated with different molecular vibrations give rise to a spectrum, that is characteristic of a specific compound" (Figure 27) [Horiba Jobin Yvon].

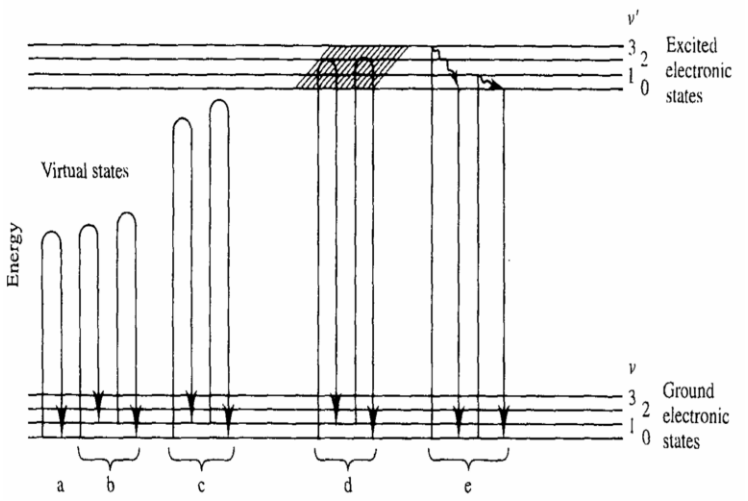

Figure 27: Mechanisms of various light-emission processes [Horiba Jobin Yvon]. The photoluminescence from the QDs is expected to be similar to resonance fluorescence like illustrated in (e) and the photoluminescence in the hexanes is assumed to be resonance Raman as illustrated in (d).

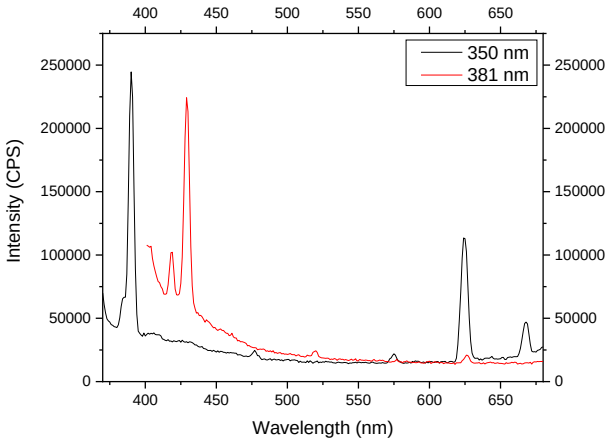

Figure 28: PL spectra of hexanes from 370-670 nm. Excitation wavelength park at two wavelengths, 350 nm and 381 nm. All characterized QDs are dispersed in hexanes and should show traces of this PL spectrum.

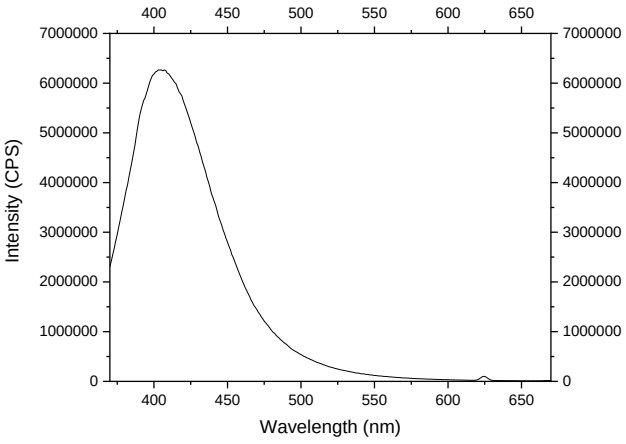

Figure 29: PL spectrum of oleylamine from 370-670 nm. Excitation wavelength park at 381 nm. All QDs should be coated in this organic ligand and should show traces of this PL spectrum.

All photoluminescence measurements of ZnTe nanoparticles, ZnTe/ZnSe QDs and ZnTe/ZnS QDs should have traces of oleylamine, an organic compound that coats the nanoparticles and functions as a stabilizing surfactant and traces of hexanes, a nonpolar organic solvent that was used to disperse the QDs superimposed on the emission from the nanoparticles. The peak of hexanes was narrow, shifted with excitation wavelength, was not attributed to photoluminescence, and was attributed to a Raman shift of the emitted photons (Figure 28); this emission is believed to be a Raman fluorescence because on the peak depends on the wavelength of excitation and shifts from the excitation peak the wavelength of excitation [Horiba Jobin Yvon]. The peak of oleylamine was broad and peaked at 407 nm when excited with 350 nm light (Figure 29).

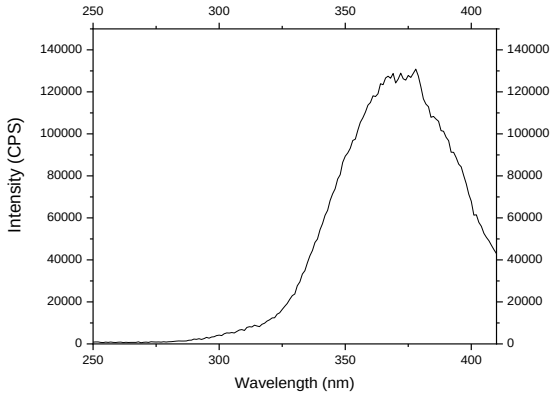

Figure 30: PL-E spectrum of ZnTe/ZnSe QDs from 250-410 nm. The excitation wavelength was scanned, and the excitation wavelength with the highest intensity is 381 nm. Emission wavelength parked at 426 nm.

The photoluminescence-excitation (PL-E) data were important because these data determine the wavelength of excitation light that will cause the QDs to emit light of the highest intensity at a fixed emission wavelength. After the PL-E measurement, with the emission monochromator parked at 426 nm, the most effective wavelength of light for excitation in photoluminescence measurements for ZnTe/ZnSe QDs was 378 nm (Figure 30). The PL-E measurements were done in conjunction with the photoluminescence measurements to optimize the photoluminescence intensity at a certain emission wavelength.

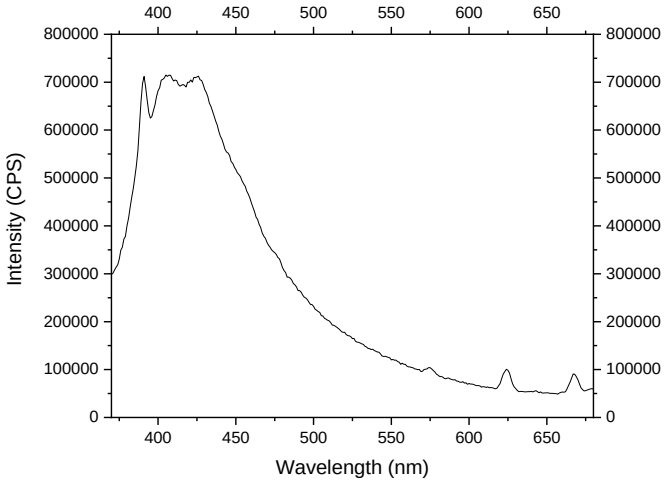

Figure 31: PL spectrum of ZnTe nanoparticles from 370-380 nm. Excitation wavelength park at 350 nm.

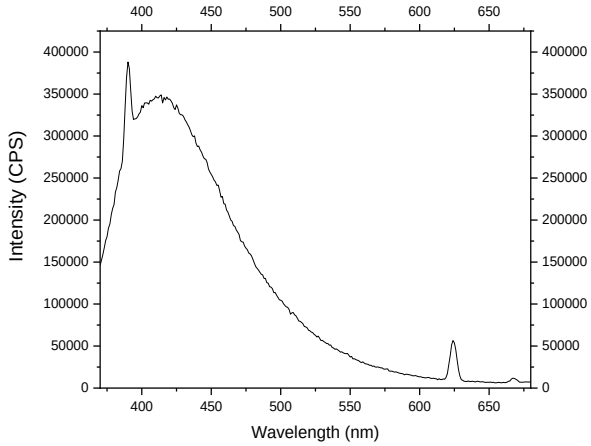

Figure 32: PL spectrum of ZnTe/ZnSe QDs from 370-680 nm. Excitation wavelength park at 381 nm.

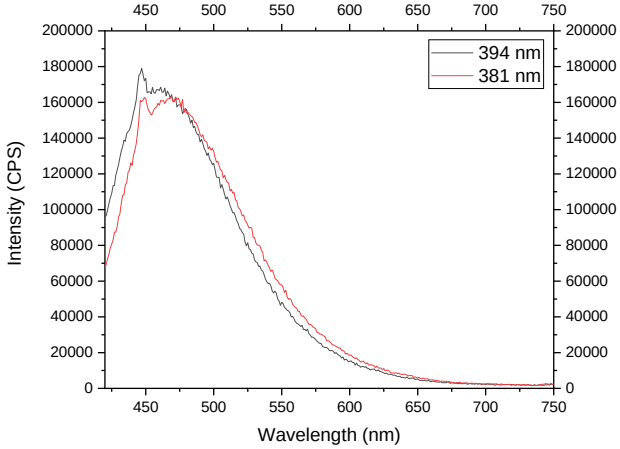

Figure 33: PL spectrum of ZnTe/ZnS QDs excited at two wavelengths from 425-750 nm.

For the ZnTe nanoparticles, we used an excitation of 350 nm. Peaks were noted in photoluminescence intensity at 391 nm, 405 nm and 426 nm. The peak at 391 nm was attributed to the hexanes (Figure 28), and the peak at 405nm is attributed to oleylamine (Figure 29), and the peak at 426 nm should be from photoluminescence of the ZnTe nanoparticles. The photoluminescence spectra of ZnTe/ZnSe QDs with an excitation wavelength of 381 nm showed

emission peaks at 391 nm, 414 nm, and 624 nm. The peak at 391 nm was from the hexanes (Figure 28), and the peak at 414 nm was a mixing of the oleylamine and nanoparticle peaks (Figure 29 and Figure 31). The 624 nm peak was present in the spectra of the ZnTe nanoparticles and the ZnTe/ZnSe QDs (Figure 31 and Figure 32).

This peak could be from the decomposition products of the nanoparticles because these peaks began to manifest in the photoluminescence spectrum a week after the synthesis. Also, it could be an amplified signal from the organics because this peak was present in the oleylamine and hexanes photoluminescence spectra (Figure 28 and Figure 29). The photoluminescence spectra of ZnTe/ZnS QDs showed a higher intensity peak when the sample was excited with a 394 nm wavelength when compared to 381 nm (the excitation wavelength that produced the peak intensity of the ZnTe/ZnSe QDs) (Figure 33).

The photoluminescence excitation spectrum was not shown for these QDs for this comparison because, at all wavelengths in the photoluminescence spectrum, the intensity was higher with an excitation of 391 nm. Because of this increase, in further photoluminescence measurements of ZnTe/ZnSe QDs an excitation wavelength of 381 nm was used, and in measurements of ZnTe/ZnS QDs an excitation wavelength of 394 nm was used because of the different sample holder.

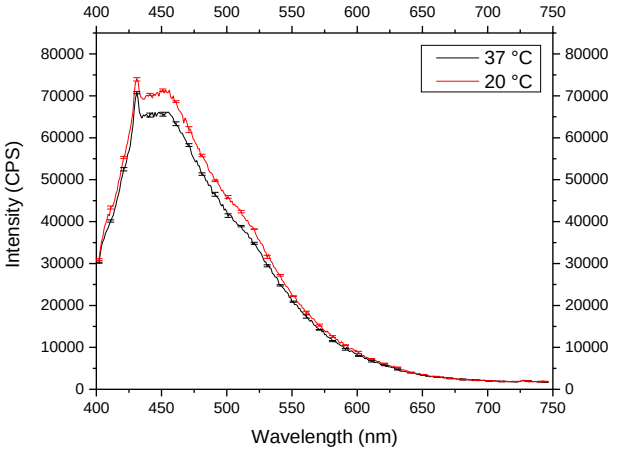

Figure 34: PL spectra of ZnTe/ZnSe QDs at room and body temperature from 400-750 nm. Excitation wavelength park at 381 nm.

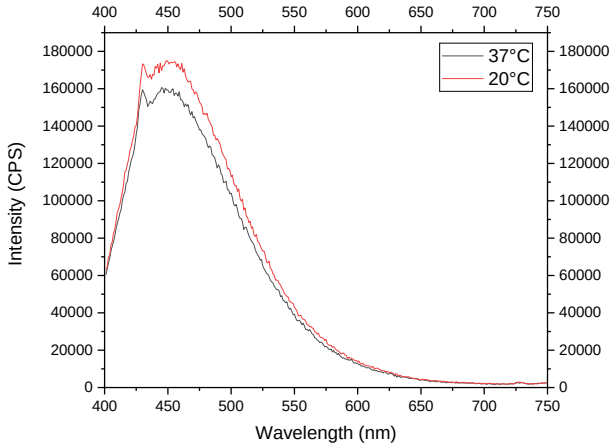

Figure 35: PL spectra of ZnTe/ZnS QDs room and body temperature from 400-750 nm. Excitation wavelength park at 394 nm.

Finally, with a sample holder that allowed for control of the temperature of the sample, photoluminescence measurements were taken in order to see how the photoluminescence intensity of the QDs varied at various temperatures. The QDs were tested at 37 ˚C, a biological temperature, to see how much the photoluminescence intensity changed from room temperature, 20 ˚C. In this test, peak photoluminescence intensity ZnTe/ZnSe (Figure 34) dropped by 4% and the peak photoluminescence intensity in the ZnTe/ZnS QDs (Figure 35) dropped by 5%. These

decreases indicate that the QDs only suffer a small loss in photoluminescence intensity at biological temperatures when compared to room temperature.

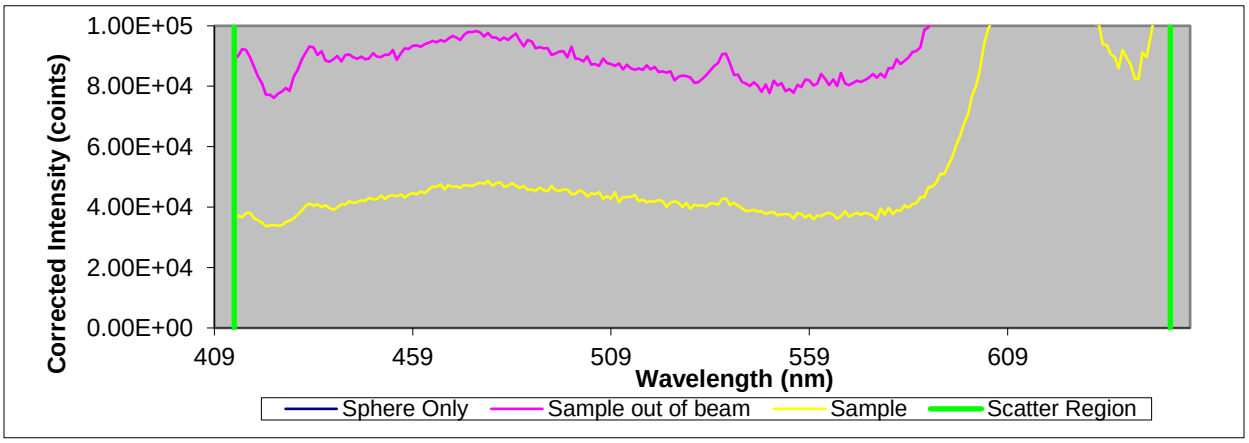

Figure 36: QY measurement of the ZnTe/ZnS QDs. The intensity of the signal at various wavelengths with the integrating sphere in various configurations is graphed and is used to calculate the photoluminescence QY.

Both samples showed poor results from the quantum yield measurements with only a 0.3% quantum yield, and both graphs looked similarly although the emission scan was from different wavelength ranges with different excitation wavelengths. The graph of the ZnTe/ZnS QDs is displayed (Figure 36). We believe these results can be improved by improving the synthesis and washing procedure to reduce the organic coating that coats the QDs after synthesis.

4. Discussion:

By understanding the characteristics of QDs, their usefulness in application may be assessed. Desirable qualities in application of QDs are a narrow size distribution, high quantum yield, long luminescence lifetime, and low cytoxicity [Wang 2013]. Also, the wavelength that the QDs emit is a function of the wavelength the QDs absorb, and the size of the nanoparticle. These are the ways to determine the quality of each QD synthesis.

Structural characterization is important in QDs because it helps develop an understanding of the physical properties such as size, size distribution and colloidal stability. All these characteristics are closely tied to the quality of luminescence of the QDs. Size of the QDs is important because it influences the wavelength of light that a material will emit when it is excited with a discrete wavelength of light. This phenomenon arises because of quantum confinement of the QDs: that is, as the size of the QDs increases so will the wavelength of light that it emits because as the size of the particles increase the effective bandgap decreases because the particles behave like a "similar to a particle in a box" [Alivisatos 1996], [Guan 2008].

The size distribution of the QDs is also important. Because the size of the particles influences the wavelength of light that is emitted, a narrow size distribution of QDs will lead a more uniform wavelength of light being emitted. This insight is valuable because, in application, QDs need to have efficient luminescence at a narrow range of wavelengths. This level of luminescence provides a predictable signal for applications such as photodynamic therapy or forester resonance energy transfer. Finally, colloidal stability, a measure of the charge on the

surface of the QDs, is an important physical property because it measures how well the particles stay in solution for extended periods of time. This measurement is valuable in application because QDs with higher stability will have longer shelf life and because they will be more viable for biomedical applications, as they will be less susceptible to degradation.

Optical characterization of QDs determines how the QDs will interact with light, and this interaction will determine the applications of the QDs. Absorption measures the intensity of absorption through a range of wavelengths, and the measurement is valuable to predict the range of light that will be used in photoluminescence characterization and to develop a method to measure a relative concentration of different samples dispersed in a similar solvent. Next, photoluminescence characterization, which measures the wavelength of light that the QDs emit with the highest intensity, is important because many variables can affect this measurement.

Throughout this project, I developed a synthesis procedure for ZnTe nanoparticle cores, and then procedures for coating the core nanoparticles with a ZnS or ZnSe shell. After each synthesis, the structural and optical properties were tested in order to optimize the procedures for the synthesis and characterization of QDs. The reported results are the most optimized synthesis procedures. The next step for optimization should be to improve the synthesis and washing procedures to leave the final product with fewer organics and improve the results from the optical and structural characterization.

The photoluminescence intensity can be improved by removing excess organic coating that absorbs the excess light and by reducing the percentage of the light that the particles can interact with. These issues in the synthesis remain that are related to the washing procedure. Anti-solvents can be found that will remove more of the organic coating from centrifugation in order to have a product with stronger photoluminescence intensity. Also, the intensity can be improved by synthesizing particles with a narrower size distribution because the particles will interact with light in a more uniform manner and they will absorb and emit the same wavelength of light to create a more defined photoluminescence peak.

From these results, we can conclude that ZnTe-based QDs are promising candidates for biomedical applications. Both samples showed good initial results from characterization. From the TEM images, the synthesis successfully created QDs composed of the intended materials. Also, the particles are absorbing ultraviolet light and are emitting visible light. Furthermore, the discussed QDs showed a less than 5% drop in peak photoluminescence intensity at biological temperatures when compared to room temperature. We observed a red shift of the light emitted when the shells were synthesized with additional shell layers. However, other issues in the synthesis, related to the washing procedure, remain to be resolved. Anti-solvents can still be found that will remove more of the organic coating from centrifugation in order to have a product with stronger photoluminescence intensity. We expect that the improved washing procedure should increase the quality of the results of the optical characterization of the QDs. With the current results, the ZnTe/ZnSe QDs appear to be the most promising candidate for biomedical applications, and the next step for this project could be to test the QDs with four shell monolayers to see if there is any improvement in the photoluminescence.

5. Acknowledgements

I gratefully acknowledge the help of the many technicians that helped him throughout this process. I would like to acknowledge Arjun Senthil and Gema Alas from the Center for High Technology Materials for the help with synthesis and laboratory procedures. I acknowledge Dr. Nathan Withers and Dr. Gennady Smolyakov from the Center for High Technology Materials for the help with laboratory procedures and guidance in writing. I acknowledge Dr. Sergei A. Ivanov and Dr. Dale L. Huber from the Center for Integrated Nanotechnologies for the help with characterization of the nanoparticles. I would also like to acknowledge the support from Dr. Lynn Beene in the process of writing the thesis. Deyannah Walker, Shruti Garude, and Mark Reymatias for help with the nanoparticle synthesis. Finally, I would like to thank Dr. Marek Osiński for the guidance in all aspects of the project,

This work was supported by the Office of Naval Research Grant N00014-18-1-2739. It was performed, in part, at the Center for Integrated Nanotechnologies, an Office of Science User Facility operated for the U.S. Department of Energy (DOE) Office of Science by Los Alamos National Laboratory (Contract DE-AC52-06NA25396) and Sandia National Laboratories (Contract DE-NA-0003525), under the Projects #2017AU0108 and #2018BU0135.

I would like to express their gratitude to Dr. Ying-Bing Jiang, Manager of the TEM/FIB Laboratory at the University of New Mexico for his assistance with TEM measurements, and to Dr. Tim Boyle of the Advanced Materials Laboratory, Sandia National Laboratories, for providing access to his colloidal synthesis laboratory and for useful discussions.

I gratefully acknowledge the support from the Maximizing Access to Research Careers Undergraduate Student Training in Academic Research (MARC U-STAR) program (NIH grant 5T34GM008751-17) and the Rayburn Reaching Up Fund from the Department of Physics and Astronomy at the University of New Mexico.

6. References

[Akins 2010] Akins, B.A., Medina, G., Memon, T.A., Rivera, A.C., Smolyakov, G.A., and Osinski, M., "Nanophosphors based on CdSe/ZnS and CdSe/SiO2 colloidal quantum dots for daylight-quality white LEDs", *CLEO/QELS: 2010 Laser Science to Photonic Applications*, pp. 1–2, 2010.

[Alivisatos 1996] Alivisatos, A.P., "Semiconductor clusters, nanocrystals, and quantum dots", *Science* **271** (5251), pp. 933–937, 1996.

[Chatterjee 2008] D. K. Chatterjee, L. S. Fong, and Y. Zhang, "Nanoparticles in photodynamic therapy: An emerging paradigm", *Advanced Drug Delivery Reviews* **60** (15), pp. 1627-1637, 2008.

[Fairclough 2012] S. M. Fairclough, E. J. Tyrrell, D. M. Graham, P. J. B. Lunt, S. J. O. Hardman, A. Pietzsch, F. Hennies, J. Moghal, W. R. Flavell, A. A. R. Watt, and J. M. Smith, "Growth and characterization of strained and alloyed type-II ZnTe/ZnSe core−shell nanocrystals", *The Journal of Physical Chemistry C* **116** (51), pp. 26898-26907, 27 Dec. 2012.

[Gonzales 2018] G. P. Gonzales, G. Alas, A. Senthil, N. J. Withers, C. Minetos, A. Sandoval III, S. A. Ivanov, G. A. Smolyakov, D. L. Huber, and M. Osiński, "Synthesis and characterization of colloidal ZnTe nanocrystals and ZnTe/ZnSe quantum dots", *Colloidal Nanoparticles for Biomedical Applications XIII* (M. Osiński, W. J. Parak, and X.-J. Liang, Eds.), SPIE International Symposium on Biomedical Optics BiOS 2018, San Francisco, CA, 27-29 Jan. 2018, *Proceedings of SPIE*, Vol. 10507, Paper 1050703, 23 Feb. 2018.

[Gonzales 2019] G. P. Gonzales, G. Alas, A. Senthil, N. J. Withers, S. A. Ivanov, G. A. Smolyakov, D. L. Huber, and M. Osiński, "Synthesis and characterization of ZnTe/ZnS quantum dots", *Colloidal Nanoparticles for Biomedical Applications XIV* (M. Osiński, A. G. Kanaras, Eds.), SPIE International Symposium on Biomedical Optics BiOS 2019, San Francisco, CA, 2 Feb. 2019, *Proceedings of SPIE*, Vol. 10892, Paper 1089206, 7 Mar. 2019.

[Guan 2008] J. A. Guan, "Synthesis and Structural Characterization of ZnTe/ZnSe Core/Shell Tunable Quantum Dots", M*assachusetts Institute of Technology*, Master Thesis, 2008.

[Hackley 2015] V. A. Hackley, "Measuring the Size of Nanoparticles in Aqueous Media Using Batch-Mode Dynamic Light Scattering", *NIST SP 1200-6*, National Institute of Standards and Technology, 2015.

[Horiba Jobin Yvon] Horiba Jobin Yvon, "Raman Application Note: Raman Scattering and Fluorescence", *Horiba Jobin Yvon*.

[Ji 2010] Ji, B., Panfil, Y.E., and Banin, U., "Heavy-metal-free fluorescent ZnTe/ZnSe nanodumbbells", *ACS Nano* **11**(7), pp. 7312–7320 (2017).

[Jing 2013] L. Jing, K. Ding, S. Kalytchuk, Y. Wang, R. Qiao, S. V. Kershaw, A. L. Rogach, and M. Gao, "Aqueous manganese-doped core/shell CdTe/ZnS quantum dots with strong fluorescence and high relaxivity", *Journal of Physical Chemistry C* **117** (36), pp. 18752-18761, 2013.

[Kim 2003] Kim, S., Fisher, B., Eisler, H.-J., and Bawendi, M., "Type-II quantum dots: CdTe/CdSe(core/shell) and CdSe/ZnTe(core/shell) heterostructures," *Journal of the American Chemical Society* **125** (38), pp. 11466–11467, 2003.

[Law 2009] W. Law, K. Yong, I. Roy, H. Ding, R. Hu, W. Zhao, W., and P. N. Prasad, "Aqueous-phase synthesis of highly luminescent CdTe/ZnTe core/shell quantum dots optimized for targeted bioimaging", *Small* **5** (11), pp. 1302-1310, 2009.

[Lincheneau 2014] C. Lincheneau, M. Amelia, M. Oszajca, A. Boccia, F. D'Orazi, M. Madrigale, R. Zanoni, R. Mazzaro, L. Ortolani, V. Morandi, S. Silvi, K. Szaciłowski, and A. Credi, "Synthesis and properties of ZnTe and ZnTe/ZnS core/shell semiconductor nanocrystals", Journal of Materials Chemistry C **2** (16), pp. 2877-2886, 2014.

[Liu 2016] X. L. Liu, D. Li, W. T. Yang, S. L. Tang, X. H. Li, L. Z. Fan, and Y. C. Li, "Controlled calcination of ZnSe and ZnTe nanospheres to prepare visible-light catalysts with enhanced photostability and photoactivity", *J Mater Sci* **51** (24), pp. 11021-11037, Dec. 2016.

[Matteucci 2006] M. E. Matteucci, M. A. Hotze, K. P. Johnston, and R. O. Williams, "Drug nanoparticles by antisolvent precipitation: Mixing energy versus surfactant stabilization", *Langmuir* **22** (21), pp. 8951- 8959, Oct. 2006.

[Patra 2016] S. K. Patra, B. Bhushan, and A. Priyam, "Water-soluble, luminescent ZnTe quantum dots: Supersaturation-controlled synthesis and self-assembly into nanoballs, nanonecklaces and nanowires", *Dalton Transactions* **45** (9), pp. 3918-3926, 2016.

[Plumley 2014] Plumley, J.B., Akins, B.A., Alas, G.J., Fetrow, M.E., Nguyen, J., Jain, P., Yang, S., Brandt, Y.I., Smolyakov, G.A., W. Ornatowski, E. D. Milligan, and M. Osiński., "Noncytotoxic Mn-doped ZnSe/ZnS quantum dots for biomedical applications", *Colloidal Nanoparticles for Biomedical Applications IX* (W. J. Parak, M. Osiński, K. I. Yamamoto, Eds.), SPIE International Symposium on Biomedical Optics BiOS 2014, San Francisco, CA, 4-6 Feb. 2014, *Proceedings of SPIE*, Vol. 8955, Paper 895513, 24 Mar. 2014.

[Qian 2009] L. Qian, D. Bera, T.-K. Tseng, and P. H. Holloway, "High efficiency photoluminescence from silica-coated CdSe quantum dots", *Applied Physics Letters* **94** (7), Art. 073112, 2009.

[Sukkabot 2015] W. Sukkabot, "Effect of ZnS shell on tight-binding simulation of zinc-blende ZnTe/ZnS core/shell nanocrystals", *Computational Materials Science* **101** (Supplement C), pp. 275-280, 2015.

[Song 2015] Y. Song, Y. Li, X. Y. Wang, X. G. Su, and Q. Ma, "Novel aqueous synthesis methods for ZnTe/ZnSe and Mn^{2+}-doped ZnTe/ZnSe type-II core/shell quantum dots", *RSC Advances* **5** (9), pp. 6271-6278, 2015.

[Tulsky 2014] E. Tulsky, J. Bartel, and J. Treadway, "Methods for preparation of ZnTe nanocrystals", *US Patent #US8637082 B2*, 28 Jan. 2014.

[Tsay 2004] J. M. Tsay, M. Pflughoefft, L. A. Bentolila, and S. Weiss, "Hybrid approach to the synthesis of highly luminescent CdTe/ZnS and CdHgTe/ZnS nanocrystals", *Journal of the American Chemical Society* **126** (7), pp. 1926-1927, 2004.

[Wang 2013] Wang, Y., Hu, R., Lin, G., Roy, I., and Yong, K.-T., "Functionalized quantum dots for biosensing and bioimaging and concerns on toxicity", *ACS Applied Materials & Interfaces* **5** (8), pp. 2786-2799, 2013.

[Wyatt 2010] Wyatt Technologies Corporation, "DYNAMICS User's Guide", *Wyatt Technologies Corporation*, p. 176, 2010.

[Xie 2005] R. Xie, X. Zhong, and T. Basché, "Synthesis, characterization, and spectroscopy of type-II core/shell semiconductor nanocrystals with ZnTe cores", *Advanced Materials* **17** (22), pp. 2741-2745, Nov. 2005.

[Xu 2010] S. Xu *et al.*, "Key roles of solution pH and ligands in the synthesis of aqueous ZnTe nanoparticles", *Chem. Mater.* **22**(21), pp. 5838-5844, Nov. 2010.

[Zhang 2006] Zhang, J., Sun, Z., and Fang, J., "Wet-chemical synthesis of ZnTe quantum dots", *MRS Online Proceedings Library Archive* 942, 2006.

[Zhao 2017] Y. Zhao, Y. Zhang, G. F. Qin, J. J. Cheng, W. H. Zeng, W., S. C. Liu, H. Kong, X. Q. Wang, Q. G. Wang, and H. H. Qu, "*In vivo* biodistribution and behavior of CdTe/ZnS quantum dots", *International Journal of Nanomedicine* **2017** (12), pp. 1927-1939, 201

Letter to the Committee:

Dear Physics Honors Thesis Committee:

Thanks to the Rayburn Reaching Up Fund and the Maximizing Access to Research Careers Program, I had the opportunity to present my research at various opportunities. I was supported by the Rayburn Reaching Up Fund through the University of New Mexico Department of Physics and Astronomy Rayburn Reaching Up Fund to attend SPIE Photonics West 2018 and 2019 and present this project at Colloidal Nanoparticles for Biomedical Applications XIII and XIV. This work was published in two proceedings from the conference.

1. G. P. Gonzales, G. Alas, A. Senthil, N. J. Withers, C. Minetos, A. Sandoval III, S. A. Ivanov, G. A. Smolyakov, D. L. Huber, and M. Osiński, "Synthesis and characterization of colloidal ZnTe nanocrystals and ZnTe/ZnSe quantum dots", *Colloidal Nanoparticles for Biomedical Applications XIII* (M. Osiński, W. J. Parak, and X.-J. Liang, Eds.), SPIE International Symposium on Biomedical Optics BiOS 2018, San Francisco, CA, 27-29 Jan. 2018, *Proceedings of SPIE*, Vol. 10507, Paper 1050703, 23 Feb. 2018.
2. G. P. Gonzales, G. Alas, A. Senthil, N. J. Withers, S. A. Ivanov, G. A. Smolyakov, D. L. Huber, and M. Osiński, "Synthesis and characterization of ZnTe/ZnS quantum dots", *Colloidal Nanoparticles for Biomedical Applications XIV* (M. Osiński, A. G. Kanaras, Eds.), SPIE International Symposium on Biomedical Optics BiOS 2019, San Francisco, CA, 2 Feb. 2019, *Proceedings of SPIE*, Vol. 10892, Paper 1089206, 7 Mar. 2019.

Also, this work was presented in various poster and oral presentations.

Invited:

1. **Gonzales, G.P.**, Alas, G., Senthil, A., Withers, N.J., Ivanov, S.A., Smolyakov, G.A., Huber, D.L. and Marek Osiński, "Synthesis and Characterization of Colloidal ZnTe/ZnSe Quantum Dots," Ringberg Seminar 2018: Matter to Life, Bavaria, Germany, December 20, 2018.

Oral:

1. **Gonzales, G.P.**, Alas, G., Senthil, A., Withers, N.J., Ivanov, S.A., Smolyakov, G.A., Huber, D.L. and Marek Osiński, "Synthesis and Characterization of Colloidal ZnTe/ZnS and ZnTe/ZnSe Quantum Dots," UNM Physics Day 2019, Albuquerque, NM, April 13, 2019.
2. **Gonzales, G.P.**, Alas, G., Senthil, A., Withers, N.J., Ivanov, S.A., Smolyakov, G.A., Huber, D.L. and Marek Osiński, "Synthesis and Characterization of Colloidal ZnTe/ZnS Quantum Dots," Proc. SPIE Photonics West, Colloidal Nanoparticles for Biomedical Applications XIV, San Francisco, CA, February 2, 2019.
3. **Gonzales, G.P.**, Alas, G., Senthil, A., Withers, N.J., Minetos, C., Sandoval, A., Ivanov, S.A., Smolyakov, G.A., Huber, D.L. and Marek Osiński, "Synthesis and Characterization of Colloidal ZnTe/ZnSe Quantum Dots," 2018 UNM Biology Research Day, Albuquerque, NM, March 23, 2018.
4. Nugyen, J.Q., Alas, G., **Gonzales, G.P.**, Minetos, C., Jaiswal, N., Sandoval, V., Sandoval, A., Ivanov, S.A., Smolyakov, G.A., Huber, D.L., Marek Osinski, "Effects of iron-oxide nanoparticles on compound biofilms of streptococcus gordonii and fusobacterium nucleatum," 2018 SPIE Photonics West: Colloidal Nanoparticles for Biomedical Applications XIII, San Francisco, CA, January 27, 2018.
5. **Gonzales, G.P.**, Alas, G., Senthil, A., Withers, N.J., Minetos, C., Sandoval, A., Ivanov, S.A., Smolyakov, G.A., Huber, D.L. and Marek Osiński, "Synthesis and characterization of colloidal ZnTe/ZnSe quantum dots," 2018 SPIE Photonics West: Colloidal Nanoparticles for Biomedical Applications XIII, San Francisco, CA, January 27, 2018.

Poster:

1. **Gonzales, G.P.**, Alas, G., Senthil, A., Withers, N.J., Ivanov, S.A., Smolyakov, G.A., Huber, D.L. and Marek Osiński, "Synthesis and Characterization of Colloidal ZnTe/ZnS and ZnTe/ZnSe Quantum Dots," UNM Undergraduate Research Opportunity Conference 2019, Albuquerque, NM, April 17, 2019.
2. **Gonzales, G.P.**, Alas, G., Senthil, A., Withers, N.J., Ivanov, S.A., Smolyakov, G.A., Huber, D.L. and Marek Osiński, "Synthesis and Characterization of Colloidal ZnTe/ZnS and ZnTe/ZnSe Quantum Dots," UNM Physics Day 2019, Albuquerque, NM, April 13, 2019.
3. **Gonzales, G.P.**, Alas, G., Senthil, A., Withers, N.J., Ivanov, S.A., Smolyakov, G.A., Huber, D.L. and Marek Osiński, "Synthesis and Characterization of Colloidal ZnTe/ZnSe Quantum Dots," 2018 SACNAS: The National Diversity in STEM Conference, San Antonio, TX, October 12, 2018.
4. **Gonzales, G.P.**, Alas, G., Senthil, A., Withers, N.J., Ivanov, S.A., Smolyakov, G.A., Huber, D.L. and Marek Osiński, "Synthesis and Characterization of Colloidal ZnTe/ZnSe Quantum Dots," 2018 Center for Integrated Nanotechnologies (CINT) Annual Meeting, Santa Fe, NM, September 24, 2018.
5. **Gonzales, G.P.**, Alas, G., Senthil, A., Withers, N.J., Ivanov, S.A., Smolyakov, G.A., Huber, D.L. and Marek Osiński, "Synthesis and Characterization of Colloidal ZnTe/ZnSe Quantum Dots," 2018 Undergraduate Research Opportunity Conference, UNM, Albuquerque, NM, April 19, 2018.
6. **Gonzales, G.P.**, Alas, G., Senthil, A., Minetos, C., Sandoval, A., Ivanov, S.A., Smolyakov, G.A., Huber, D.L. and Marek Osiński, "Synthesis and Characterization of Luminescent ZnTe-Core Quantum Dots," 2017 SACNAS: The National Diversity in STEM Conference, Salt Lake City, OH, October 20, 2017.
7. **Gonzales, G.P.**, Alas, G., Senthil, A., Minetos, C., Sandoval, A., Ivanov, S.A., Smolyakov, G.A., Huber, D.L. and Marek Osiński, "Synthesis and Characterization of Luminescent ZnTe-Core Quantum Dots," 2017 UNM Summer Biomedical Research Symposium, Albuquerque, NM, August 11, 2017.

Other (3minute Pitch):

1. **Gonzales, G.P.**, Withers, N.J., and Marek Osiński, "Iron oxide nanoparticles for antimicrobial applications," UNM Undergraduate Research Opportunity Conference (UROC) 2019, Albuquerque, April 18, 2019.

Awards:

1. UNM UROC 180: Third Place (pitch competition)
2. UNM Physics Day 2019: Best Poster Presentation Prize

Sincerely,

Gavin Gonzales